Bounds for shakedown of cohesive-frictional materials under moving surface loads

Jidong Zhao *, Scott W. Sloan, Andrei V. Lyamin, Kristian Krabbenhøft

Centre for Geotechnical and Materials Modelling, The University of Newcastle, University Drive, Callaghan, NSW 2308, Australia

Abstract

In this paper, shakedown of a cohesive-frictional half space subjected to moving surface loads is investigated using Melan's static shakedown theorem. The material in the half space is modelled as a Mohr–Coulomb medium. The sliding and rolling contact between a roller and the half space is assumed to be plane strain and can be approximated by a trapezoidal as well as a Hertzian load distribution. A closed form solution to the elastic stress field for the trapezoidal contact is derived, and is then used for the shakedown analysis. It is demonstrated that, by relaxing either the equilibrium or the yield constraints (or both) on the residual stress field, the shakedown analysis leads to various bounds for the elastic shakedown limit. The differences among the various shakedown load factors are quantitatively compared, and the influence of both Hertzian and trapezoidal contacts for the half space under moving surface loads is studied. The various bounds and shakedown limits obtained in the paper serve as useful benchmarks for future numerical shakedown analysis, and also provide a valuable reference for the safe design of pavements.
© 2008 Elsevier Ltd. All rights reserved.

Keywords: Shakedown; Cohesive-frictional materials; Cyclic load; Hertzian contact; Trapezoidal contact; Analytical solution; Pavement design

1. Introduction

The static shakedown theorem proposed by Melan (1938), together with the kinematic shakedown theorem proposed by Koiter (1960), constitute the cornerstone of shakedown analysis for elastoplastic structures under cyclic loading. While originally used to address material behaviour with simple assumptions such as geometric linearity, elastic perfectly plastic constitutive relations and associated flow, the shakedown theorems have been extended to cover a broad category of applications that account for the effects of high temperature, strain or work hardening, nonlinear geometry, dynamic behaviour, and non-associated plastic flow. Numerical methods such as the finite element method have also been employed to predict shakedown behaviour in various materials for general cases. Shakedown theory has thus become a useful tool in the design of a wide range

---

of practical applications such as railway foundations, pavement engineering, roller bearings, and the machining industry. Comprehensive reviews of the development of shakedown theory can be found in various monographs such as those of König and Maier (1981), Polizzotto (1982), Johnson (1985) and König (1987), as well as more recent research papers (see, for example, Ponter et al., 1985, 2006; Pycko and Maier, 1995; Maier, 2001; Polizzotto et al., 2001; Zouain and Silveira, 2001; Bousshine et al., 2003; Feng and Sun, 2007; Polizzotto, 2007; Pham, 2007 and references therein).

In pavement engineering, the evaluation of road performance requires proper assessment of the permanent deformation and fatigue under moving traffic loads. The complex nature of the problem clearly requires accurate theoretical models in order to simulate the actual failure mechanics observed in pavement engineering (Brown, 1996). In practice, it is economically desirable to construct pavements that can sustain stress levels well beyond the elastic limit of their constituent materials. In particular, it is of major importance to determine whether a given pavement structure, when subjected to a large number of load cycles, will experience progressive accumulation of plastic strains and gradual failure, or whether the increase in plastic strains will cease to occur, thereby leading to a stable response or shakedown. Field observations indicate that many pavements do in fact shakedown rather than deform continuously. The use of the shakedown theorems can thus enable the long term behaviour of a pavement to be determined without resorting to computationally expensive step-by-step analyses. As a consequence, shakedown theory has received much attention from researchers in the field of pavement engineering over the past two decades – see, for example, the work of Sharp and Booker (1984), Collins and Cliffe (1987), Collins et al. (1993), Yu and Hossain (1998), Collins and Boulbibane (2000), Yu (2005) and Krabbenhøft et al. (2007a).

For a given structure and load regime, the shakedown load factor depends on the elastic parameters and the yield limits of the materials, not on the actual way the system evolves before the shakedown condition is reached (Martin, 1975; Stein et al., 1992). In order for shakedown theory to provide useful pavement design information, the Mohr–Coulomb yield criterion has long been preferable to the Tresca criterion for the description of the cohesive-frictional nature of pavement materials, but this gives rise to a number of complications in analytical and numerical computations. Sharp and Booker (1984) proposed an elegant method of conics to handle Mohr–Coulomb materials in shakedown analysis. This was studied further by Collins and Cliffe (1987) in conjunction with kinematic upper bounds for the shakedown limit. The finite element method, in tandem with linear and nonlinear programming techniques, has also been used to compute shakedown limits numerically (see, e.g., Shiau, 2001; Boulbibane and Ponter, 2006; Li and Yu, 2006). When applying Melan's theorem to cohesive-frictional materials, however, considerable confusion exists that may give rise to inaccurate and inconsistent predictions of the shakedown limit. Specifically, some of the constraints on the residual stresses that are necessary in deriving rigorous shakedown limits are often inadvertently neglected. As pointed out by Krabbenhøft et al. (2007a), and demonstrated again here, this always leads to upper bounds to the static shakedown limit.[1]

The *first* constraint that is frequently neglected in the literature is *the yield condition* on the residual stress field. According to Melan's theorem, this constraint is necessary in deriving the shakedown limit for cyclic loading of a pavement. For such a pavement, the moving loads on the road surface constitute a typical two-point load domain with zero being one of the load vertices. Once the external load becomes zero, the yield constraint on the combined (total) stresses in Melan's theory will degenerate to a yield constraint on the residual stresses alone. Thus, to ensure the whole stress history lies within the yield surface, the yield constraint must be imposed on the residual stresses. One may argue that by checking the yield condition on the total stresses this scenario should be covered automatically as a special case. Depending on the procedure used to compute the shakedown limit, this is not always sufficient (as discussed in detail in Section 4). Research that recognises this key point in pavement shakedown analysis includes the work of Sharp and Booker (1984), Collins and Cliffe (1987) and Krabbenhøft et al. (2007a). Collins and Cliffe (1987) appear to be the first to explicitly indicate that the residual stresses must satisfy the yield condition when computing the shakedown limit. They remark that the *positive* shakedown load factor must be obtained with *a residual stress that lies between the uniaxial compression and tension limits*. This requirement is precisely the yield constraint on the

---

[1] Provided an exact elastic solution is employed and the discretisation error is small.

residual stress field for the special case of plane strain rolling contact on a cohesive-frictional material. The *second* key constraint arises from *the equilibrium condition* on the residual stresses. For cohesive-frictional materials, the introduction of the Mohr–Coulomb criterion in shakedown analysis complicates the derivation of analytical solutions and numerical approaches appear to be the only option. In the plane strain rolling contact problem treated here, we will demonstrate that the equilibrium condition on the residual stresses can be easily missed in a numerical computation, and that the resultant load factor often overestimates the true shakedown limit.

The main purpose of this paper is to demonstrate the significance of the above-mentioned residual stress constraints when predicting shakedown limits. To this end, an example of a half space under moving surface loads is studied for the case of rolling and sliding contact between a roller and road surface. Both Hertzian and trapezoidal load distributions are investigated. By neglecting either or both of the two constraints on the residual stresses, we show that various bounds to the static shakedown limit are obtained. If they are used for pavement applications, these solutions may thus lead to unconservative designs. When deriving a rigorous static shakedown limit, the exact elastic stress distribution in the half space under the contact load is needed. While the solution to the Hertzian contact problem was solved last century, it is surprising to find that a closed form solution for trapezoidal rolling and sliding contact is not available in the literature. Even though many have referred to the monograph of Poulos and Davis (1974), they only give solutions for a special case. This paper thus derives a general closed form solution to the trapezoidal rolling and sliding contact problem. In this solution, the trapezoidal shape is variable (compared with the fixed geometry given in the past) so that various contact shapes between a roller and the road surface can be simulated. The exact solution to the trapezoidal contact problem is useful in other applications, such as benchmarking elastic stress fields computed by finite elements. It is shown that the shakedown limits obtained using this exact elastic solution are quite different to those given in previous studies. Possible reasons for this discrepancy are discussed.

2. Shakedown and the constraints on the residual stress field

Residual stress is a tensile or compressive stress which exists in the bulk of a material without application of an external load. Melan's shakedown theorem states that these stresses must be time-independent, self-equilibrating and satisfy the yield constraint in order for shakedown to occur. Suppose a structure is subjected to a cycle of loading and unloading. Upon removal of all external forces and displacements at the end of the cycle, we consider the material body to be in an intermediate 'stable' state, where 'stable' is used to imply that plastic flow (if any) ceases to occur and a rate-independent state exists in the structure. According to Koiter (1960), no more than one residual stress distribution can exist in the material body given this intermediate stable state of plastic strains (and zero prescribed displacements on some surface S_u). To ensure this intermediate stable deformation state is time-independent, the corresponding residual stress field must therefore nowhere violate the yield condition otherwise plastic flow will continue to occur. This point has been emphasized by Symonds (1951) in an alternative proof of Melan's shakedown theorem. To summarise the above points, Melan's static shakedown theorem may be expressed mathematically in the following form:

$$\lambda_{SD} = \max_{(\lambda, \boldsymbol{\rho})} \lambda \text{ s.t.} \begin{cases} \rho_{ij,j} = 0, \quad n_i \rho_{ij} = 0, \\ f(\rho_{ij}) \leqslant 0, \\ f(\rho_{ij} + \lambda \sigma_{ij}) \leqslant 0. \end{cases} \tag{1}$$

where λ is the load factor, ρ_{ij} is a self-equilibrating residual stress field, σ_{ij} is an elastic stress field induced by cyclic external loads, $f(\cdot)$ denotes the yield condition, and λ_{SD} is the 'static shakedown limit'. For each stage of loading, the sum of the elastic stress and the residual stress, $\hat{\sigma}_{ij} = \rho_{ij} + \sigma_{ij}$, is termed the 'post transient stress' by Polizzotto (1993). Note that in Eq. (1), the first two equations denote the self-equilibrating conditions, while the last two inequalities denote the yield conditions on the residual stresses and total stresses, respectively. These two yield conditions guarantee that both the residual stresses and the total stresses are 'safe stresses' as termed by Koiter (1960).

While both the self-equilibrium and yield constraints are necessary to ensure that shakedown occurs, there are some interesting implications if either or both of them are neglected in the calculation of the shakedown limit. First, if we neglect both the equilibrium and yield constraints on the residual stresses, Eq. (1) simplifies to:

$$\lambda_I = \max_{(\lambda, \rho_{ij})} \lambda \ \text{s.t.} f(\rho_{ij} + \lambda\sigma_{ij}) \leqslant 0. \tag{2}$$

which will constitute an upper bound on the static shakedown limit. Following Krabbenhøft et al. (2007a), we denote this load factor an "upper bound type 1" for convenience. Relaxing all the specific constraints on the residual stresses ρ_{ij} means that they may assume many values, including ones which cancel the stresses induced by the external loads to make the total stresses lie within the yield surface. As a consequence, the "upper bound type 1" solutions defined in Eq. (2) can, theoretically, be infinite. However, for the sliding and rolling contact problem considered here, the residual stresses ρ_{ij} are properly bounded so that the upper bound type 1 solution still has a finite value.

Alternatively, if we relax the equilibrium conditions on the residual stress field but retain the yield conditions, another upper bound to the static shakedown limit can be obtained:

$$\lambda_{II} = \max_{(\lambda, \rho_{ij})} \lambda \ \text{s.t.} \begin{cases} f(\rho_{ij}) \leqslant 0, \\ f(\rho_{ij} + \lambda\sigma_{ij}) \leqslant 0. \end{cases} \tag{3}$$

This load factor will be termed an "upper bound type 2" on the static shakedown limit. We note that this upper bound actually corresponds to the static plastic shakedown limit as defined by Polizzotto (1993). The relationship of the plastic shakedown limit to other shakedown limits, for a variety of deviatoric plastic models, has been discussed by Krabbenhøft et al. (2007b).

Finally, a third type of upper bound on the elastic shakedown limit can be obtained by relaxing the yield constraints on the residual stress field but retaining the equilibrium conditions:

$$\lambda_{III} = \max_{(\lambda, \rho)} \lambda \ \text{s.t.} \begin{cases} \rho_{ij,j} = 0, \quad n_i\rho_{ij} = 0, \\ f(\rho_{ij} + \lambda\sigma_{ij}) \leqslant 0. \end{cases} \tag{4}$$

As the elastic stress field σ_{ij} is in equilibrium, the above factor actually corresponds to the plastic collapse load that is often treated in limit analysis. In this paper, we term it an 'upper bound type 3'. Provided σ_{ij} is exact and the discretisation error is small, we expect the shakedown limits described above to be ordered so that $\lambda_E \leqslant \lambda_{sd} \leqslant (\lambda_{II}, \lambda_{III}) \leqslant \lambda_I$, where λ_E denotes the elastic limit.

3. Rolling and sliding contact between a vehicle wheel and pavement

3.1. Contact approximations

To begin with, the material of the half space is assumed to be isotropic and homogeneous, with a self-weight which is small compared to the stress gradient being applied so that it can be neglected. As remarked by Sharp and Booker (1984), analysing the behaviour of a pavement subjected to wheel loads is by no means trivial since the latter are cyclic and vary in magnitude, contact area and spatial distribution. Indeed, the problem is sufficiently complex that one has to resort to appropriate simplifications. A commonly used approximation of the actual wheel loading is to simulate it as a roller loading with the axis of the roller being normal to the travel direction (x) and the vertical direction (z). Under these conditions, the problem can be simplified to be a two-dimensional plane strain one with the out-of-plane axis coinciding with the wheel axis. The resulting stress state in the vertical plane $y - z$ through the centreline of the wheel is simulated with reasonable accuracy, while the stresses in other regions are generally overestimated (thus implying a conservative estimation of the true load limits for the pavement). The roller load is assumed here to traverse the surface $z = 0$ of the half space continuously in the x direction. The coefficient of friction μ between the tyre and the road surface is assumed to be constant, with the slip between the roller and the road surface being fully developed so that the tangential shear loading is proportional to the vertical pressure.

Experimental studies (e.g., Freitag and Green, 1962) have shown the normal stresses due to a pneumatic tyre exhibit a variation in the direction of travel which can be approximated by a trapezoidal distribution (Fig. 1b). Indeed, this pressure distribution has been assumed in many previous shakedown analyses in combination with an independent horizontal shear stress induced by friction (e.g., Sharp and Booker, 1984; Collins and Cliffe, 1987 among others). Approximating the rolling–sliding contact by a trapezoidal pressure distribution is appealing for numerical computations, since it is simple to model. However, it can be argued that the real contact pressure distribution between a loaded tyre and the road surface should be smoothly continuous across the contact area. This leads to another popular approximation, Hertzian contact (Johnson, 1985), for simulating rolling and sliding behaviour on pavements (Fig. 1a). One major advantage of the Hertzian approximation is the availability of an exact analytical solution for the elastic stress field. Nevertheless, we note that the shape of the actual contact depends heavily on the tyre inflation pressure as well as the magnitude of the load. According to Croney (1977), when the load is small or the inflation pressure is high, the contact area is approximately circular. Otherwise, if the wheel load is high or the tyre inflation pressure is low, the contact area becomes elongated (see Fig. 2). If we assume the design tyre has the same standard inflation pressure, shakedown analysis seeks the highest load a pavement can sustain and an elongated contact area is more appropriate. Thus a trapezoidal pressure distribution with a high b/a ratio will be physically more realistic than a Hertzian distribution. Nevertheless, in this paper, we investigate both cases and present comparisons between the results.

To simulate the contact behaviour between a tyre and the road surface under extreme cyclic loads realistically, a trapezoidal pressure distribution with a b/a value greater than 0.9 may be necessary (see Fig. 2). In the majority of previous shakedown studies dealing with trapezoidal contact, however, this ratio has been fixed at 0.5. As will be shown later, assuming $b/a = 0.5$ will often lead to a static shakedown limit that is greater than those for higher values of b/a. This effect may possibly lead to unsafe pavement design and will
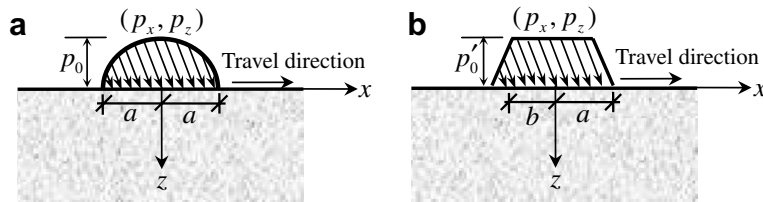
Fig. 1. Definitions of pavement surface subject to rolling and sliding loading. (a) Hertzian contact; (b) trapezoidal contact.
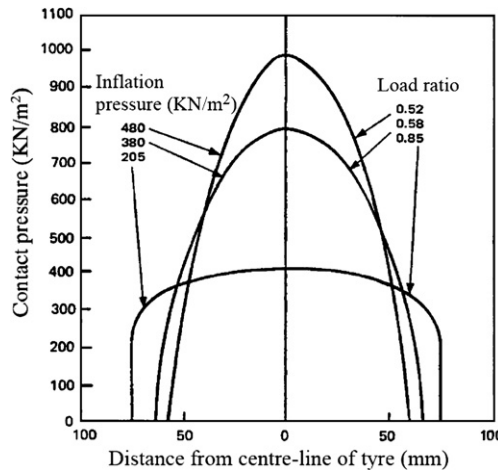
Fig. 2. Lateral contact pressure measure between loaded tyre and road surface (after Croney, 1977).

be studied by presenting shakedown limits for a variety of b/a ratios. To obtain these limits, a new solution for the elastic stress field in the half space underneath a general trapezoidal contact pressure distribution is derived. Somewhat surprisingly, no closed form solution to the exact elastic stress field appears to have been given for the frictional contact case with a variable ratio of b/a. Following the convention in soil mechanics, compressive stresses are taken to be positive in this paper.

3.2. Analytical elastic stress solutions to the contact problem

For the Hertzian contact, the pressure distribution due to the moving roller is given by the following expressions:

$$\begin{cases} p_z = p_0 \sqrt{1 - (x/a)^2} \\ p_x = \mu p_z \end{cases} \tag{5}$$

where p_0 denotes the maximum vertical pressure at $x = 0$ (see Fig. 1a). To make the trapezoidal distribution comparable to the Hertzian one, we assume the half contact lengths, a, for the two cases are the same, but b is left unspecified. Suppose the maximum vertical pressure at the centre of the trapezoid is p'_0 (see Fig. 1b). Then the pressure distribution for the trapezoidal case is:

$$\begin{cases} p_z = p'_0(a - |x|)/(a - b), & b < |x| \leqslant a; \\ p_z = p'_0, & |x| \leqslant b; \\ p_x = \mu p_z. \end{cases} \tag{6}$$

In addition, we need to set the total vertical force in both cases to be equal so that:

$$\int_{-a}^{a} p_0 \sqrt{1 - (x/a)^2}\, dx = F_z = \int_{-b}^{b} p'_0\, dx + 2 \int_{b}^{a} p'_0 \frac{a - x}{a - b}\, dx \tag{7}$$

This gives the following relation between p_0 and p'_0:

$$p'_0 = \frac{\pi a}{2(a + b)} p_0 \tag{8}$$

Therefore, for the trapezoidal distribution, we have:

$$\begin{cases} p_z = \pi a p_0(a - |x|)/[2(a^2 - b^2)], & b < |x| \leqslant a; \\ p_z = \pi a p_0/[2(a + b)], & |x| \leqslant b; \\ p_x = \mu p_z. \end{cases} \tag{9}$$

The elastic stresses in the half space for Hertzian contact can be found in Johnson (1985) and will not be repeated here. As there is no closed form solution available in the literature for the general trapezoidal contact case, we derive one in this paper. Following the procedure proposed by Johnson (1985), integrating the point vertical force and horizontal traction over the contact area gives the following elastic stress solution (for detailed derivations see the Appendix A):

$$\begin{cases} \sigma_{xx} = \frac{p'_0}{\pi(a-b)} \left\{ z \ln \left(\frac{R_2^2}{R_3^2} \frac{R_4^2}{R_1^2} \right) + (x + a)\alpha_3 - (x - a)\alpha_1 + (a - b)\alpha_2 \right\} \\ \qquad + \frac{\mu p'_0}{\pi(a-b)} \left\{ 3z(\alpha_3 - \alpha_1) + (x - a)\ln \left(\frac{R_1^2}{R_2^2} \right) - (x + a)\ln \left(\frac{R_2^2}{R_4^2} \right) - (a - b)\ln \left(\frac{R_2^2}{R_3^2} \right) \right\} \\ \sigma_{zz} = \frac{p'_0}{\pi(a-b)} \left\{ (x + a)\alpha_3 + (a - b)\alpha_2 - (x - a)\alpha_1 \right\} + \frac{z\mu p'_0}{\pi(a-b)} \left\{ \alpha_1 - \alpha_3 \right\} \\ \sigma_{xz} = \frac{z p'_0}{\pi(a-b)} \left\{ \alpha_1 - \alpha_3 \right\} + \frac{\mu p'_0}{\pi(a-b)} \left\{ z \ln \left(\frac{R_2^2}{R_4^2} \frac{R_3^2}{R_1^2} \right) + (x + a)\alpha_3 - (x - a)\alpha_1 + (a - b)\alpha_2 \right\} \end{cases} \tag{10}$$

where the definitions for α_i ($i = 1, 2, 3$) and R_i ($i = 1, \ldots, 4$) are shown in Fig. 3.

At the pavement surface, $z = 0$, $R_1^2 = (x - a)^2$, $R_2^2 = (x - b)^2$, $R_3^2 = (x + b)^2$, and $R_4^2 = (x + a)^2$. The surface stress distribution then has the following forms:

(1) $|x| > a$

In this case, $\alpha_1 = \alpha_2 = \alpha_3 = 0$ and:

$$
\begin{cases}
\sigma_{xx} = \frac{\mu p_0'}{\pi(a-b)} \left\{ (x-a)\ln\left(\frac{x-a}{x-b}\right)^2 - (x+a)\ln\left(\frac{x+b}{x+a}\right)^2 - (a-b)\ln\left(\frac{x-b}{x+b}\right)^2 \right\}, \\
\sigma_{zz} = 0, \quad \sigma_{xz} = 0.
\end{cases}
\tag{11}
$$

(2) $b \leqslant |x| \leqslant a$

In this case, $\alpha_2 = 0$. When $b \leqslant x \leqslant a$, then $\alpha_1 = \pi$ and $\alpha_3 = 0$. If $-a \leqslant x \leqslant -b$, then $\alpha_3 = \pi$ and $\alpha_1 = 0$. Generally, if $b < |x| < a$, we have:

$$
\begin{cases}
\sigma_{xx} = \frac{(a-|x|)p_0'}{(a-b)} + \frac{\mu p_0'}{\pi(a-b)} \left\{ (x-a)\ln\left(\frac{x-a}{x-b}\right)^2 - (x+a)\ln\left(\frac{x+b}{x+a}\right)^2 - (a-b)\ln\left(\frac{x-b}{x+b}\right)^2 \right\}, \\
\sigma_{zz} = \frac{(a-|x|)p_0'}{(a-b)}, \quad \sigma_{xz} = \frac{(a-|x|)\mu p_0'}{(a-b)}.
\end{cases}
\tag{12}
$$

At $x = \pm a$, either $(x-a)\ln\left(\frac{x-a}{x-b}\right)^2 = 0$ or $(x+a)\ln\left(\frac{x+a}{x+b}\right)^2 = 0$. We thus have:

$$
\begin{cases}
\sigma_{xx} = -\frac{sign(x)\mu p_0'}{\pi(a-b)} \left\{ 2a\ln\left(\frac{a+b}{2a}\right)^2 + (a-b)\ln\left(\frac{a-b}{a+b}\right)^2 \right\}, \\
\sigma_{zz} = 0, \quad \sigma_{xz} = 0.
\end{cases}
\tag{13}
$$

Similarly, at $x = \pm b$, we have:

$$
\begin{cases}
\sigma_{xx} = p_0' - \frac{sign(x)\mu p_0'}{\pi(a-b)} \left\{ (a-b)\ln\left(\frac{b-a}{2b}\right)^2 + (b+a)\ln\left(\frac{2b}{b+a}\right)^2 \right\}, \\
\sigma_{zz} = p_0', \quad \sigma_{xz} = \mu p_0'.
\end{cases}
\tag{14}
$$

(3) $|x| < b$

In this case, $\alpha_2 = \pi$, $\alpha_1 = \alpha_3 = 0$ and:

$$
\begin{cases}
\sigma_{xx} = p_0' + \frac{\mu p_0'}{\pi(a-b)} \left\{ (x-a)\ln\left(\frac{x-a}{x-b}\right)^2 - (x+a)\ln\left(\frac{x+b}{x+a}\right)^2 - (a-b)\ln\left(\frac{x-b}{x+b}\right)^2 \right\}, \\
\sigma_{zz} = p_0', \quad \sigma_{xz} = \mu p_0'.
\end{cases}
\tag{15}
$$

3.3. Mohr–Coulomb yield criterion for the pavement soil

The Mohr–Coulomb criterion is used to model the pavement under plane strain conditions:

$$
f(\sigma_{xx}, \sigma_{zz}, \sigma_{xz}) = \sqrt{(\sigma_{zz} - \sigma_{xx})^2 + 4\sigma_{xz}^2} - (\sigma_{zz} + \sigma_{xx})\sin\phi - 2c\cos\phi = 0
\tag{16}
$$

where c is the cohesion, ϕ is the internal friction angle, and the soil mechanics convention of compression being positive applies.
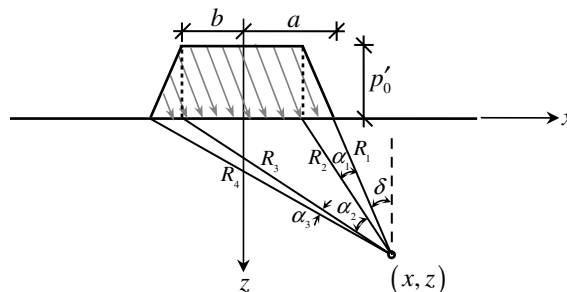

Fig. 3. Illustration of the trapezoidal contact.

4. Solution procedures and shakedown results

4.1. Solution procedures

For the rolling and sliding contact problem, the permanent deformation and residual stress distribution for the plane strain contact will be independent of x and depend only on the depth z. The equilibrium of the residual stresses thus implies that there is only non-zero component ρ_{xx}, which is a function of z only. In view of this, the yield condition on the *total* stresses for the plane strain half space is:

$$f(\lambda\sigma_{ij}, \rho_{xx}) = \sqrt{(\lambda\sigma_{zz} - \lambda\sigma_{xx} - \rho_{xx})^2 + 4\lambda^2\sigma_{xz}^2} - (\lambda\sigma_{zz} + \lambda\sigma_{xx} + \rho_{xx})\sin\phi - 2c\cos\phi = 0 \tag{17}$$

By setting $\partial f/\partial\rho_{xx} = 0$, we can find the following optimal residual stress *without any constraint*:

$$\rho_{xx}^* = 2c\tan\phi + \lambda\left(\sigma_{xx} - \frac{1 + \sin^2\phi}{\cos^2\phi}\sigma_{zz}\right) \tag{18}$$

and the corresponding load factor is (see, also, Collins and Cliffe, 1987; Yu, 2005):

$$\lambda = \frac{c}{|\sigma_{xz}| - \sigma_{zz}\tan\phi} \tag{19}$$

If we impose the yield constraint on the residual stress by enforcing $f(\rho_{xx}) = 0$, we obtain the following two bounds for ρ_{xx}:

$$\begin{cases} \rho_{xx}^+ = -2c\tan\left(\frac{\phi}{2} - \frac{\pi}{4}\right) \\ \rho_{xx}^- = -2c\tan\left(\frac{\phi}{2} + \frac{\pi}{4}\right) \end{cases} \tag{20}$$

where ρ_{xx}^+ and ρ_{xx}^- are the compressive and tensile strength limits of the soil, respectively.

The static shakedown limit and the various upper bounds except type 3 can be computed according to the procedures outlined by Krabbenhøft et al. (2007a) for Hertzian contact. Alternatively, we can employ the method of conics, proposed initially by Sharp and Booker (1984) and later elaborated on by Collins and Cliffe (1987), to find the various shakedown limits. As remarked by Collins and Cliffe (1987), the yield equation for each material point Eq. (17) is a conic in terms of λ and ρ_{xx}. Depending on the sign of the quantity $s = |\sigma_{xz}| - \sigma_{zz}\tan\phi$, it can be an ellipse ($s > 0$) ($p_1$, p_2 and p_3 in Fig. 4 for instance), a parabola ($s = 0$), or a hyperbola ($s < 0$). For the last two cases, the resultant load factor is either infinite or negative, so that the corresponding material element is usually not the critical point we are after. We thus use the case where all conics are ellipses in the following demonstration. From the form of Eq. (17), it is readily seen that the ellipses for all material points will pass through two-points, $(\rho_{xx}^+, 0)$ and $(\rho_{xx}^-, 0)$, in the plane of ρ_{xx} and λ (see Fig. 4). We next assume the half space is divided into a grid by a series of infinitely-long horizontal lines at depths ($z_j, j = 1, 2, \ldots$) and a series of semi-infinite vertical lines at locations ($x_i, i = 1, 2, \ldots$). Each material element is denoted by an intersecting point of these lines, such as the points p_1, p_2 and p_3 as shown in Fig. 4.

(1) *Upper bound type 1*: To determine the upper bound type 1 load factor, we need first to find the corresponding optimal load factor that satisfies Eq. (2) at each material point in each layer. This is determined by the corresponding λ of the top-most point of each conic, for example, λ_A for p_2, λ_B for p_1, and λ_C for p_3 in Fig. 4. These points can be found from the differential of Eq. (17) with respect to ρ_{xx} through Eqs. (18) and (19). We then record the smallest positive λ value, λ_I, of all the load factors $\lambda^{(i,j)}$ in the half space as the one corresponding to the upper bound type 1 (e.g., λ_A amongst λ_A, λ_B and λ_C in Fig. 4). We note, however, that for the moving contact problem being treated here, ρ_{xx} is the only non-zero component of the residual stress field that is independent of x and the equilibrium condition has actually been used once. Strictly speaking, the shakedown load factor derived here is not the one as defined in Eq. (2). Nevertheless, it is still an upper bound on the static shakedown limit and we will call it an 'upper bound type 1' in this paper.

(2) *Upper bound type 2*: Now if we impose the yield constraint on the residual stresses as well as the conditions for the above case, we obtain a load factor of upper bound type 2, λ_{II}. To find this quantity, we first obtain the optimal load factor at each material point according to Eq. (19), and then check if the correspond-
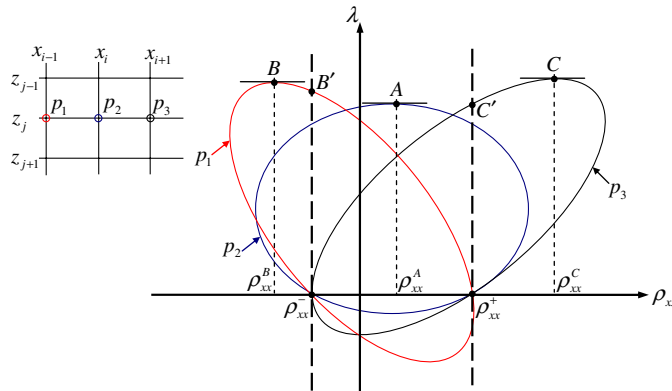
Fig. 4. Schematic illustration of determination of shakedown limit and its upper bounds by conics.

ing optimal residual stress ρ_{xx}^*, as defined in Eq. (18), falls within the range bounded by ρ_{xx}^+ and ρ_{xx}^- in Eq. (20). Referring to Fig. 4 for material point p_2, the corresponding optimal residual stress $\rho_{xx}^A \in [\rho_{xx}^-, \rho_{xx}^+]$, so that λ_A is a valid optimal load factor satisfying Eq. (3). In contrast, for material points p_1 and p_3, neither ρ_{xx}^B nor ρ_{xx}^C is within the range $[\rho_{xx}^-, \rho_{xx}^+]$ so that λ_B and λ_C are invalid load factors. In this case, we need to choose the largest λ from the two intersection points of the conics with the two vertical boundary lines $\rho_{xx} = \rho_{xx}^+$ and $\rho_{xx} = \rho_{xx}^-$. For p_1 and p_3, we see from Fig. 4 that the corresponding load factor can be obtained as $\lambda_{B'}$ and $\lambda_{C'}$, respectively. Once the load factors for all material points are obtained as described above, the corresponding load factor for an upper bound type 2, λ_{II}, is the minimum amongst them.

(3) *Static shakedown limit:* To determine the static shakedown limit defined in Eq. (1), we have to enforce the equilibrium conditions as well as the constraints for an upper bound type 2 solution. This implies that the residual stress ρ_{xx} for the corresponding load factor has to be uniform for each layer ($\partial \rho_{xx}/\partial x = 0$). As an illustrative demonstration, some typical cases are presented in Fig. 5(a–c). If the minimum load factor λ_A and the corresponding optimal residual stress $\rho_{xx}^A \in [\rho_{xx}^-, \rho_{xx}^+]$ give stresses at all other material points that lie within or on the yield surface (case Fig. 5a), then λ_A is the load factor we need to record for this layer. Otherwise, if λ_A and ρ_{xx}^A violate the yield condition at some material points (as shown in Fig. 5b and c), we need to find the intersection point of these conics with the largest load factor, such as point A' in Fig. 5b and c, and record this. The static shakedown limit is then given as the minimum load factor for all layers. In practical numerical computations, it is too laborious to search for the static shakedown limit in the above way. Instead, we employ a 'scanning line' method as shown in Fig. 5d. This method divides the range of $[\rho_{xx}^-, \rho_{xx}^+]$ into a series of fine scanning lines ρ_{xx}^k, where each scanning line corresponds to a residual stress. For each scanning line and layer, we solve the yield Eq. (17) at each material point for a positive λ. The minimum for all such points is recorded as the optimal load factor, $\lambda_{\rho z}$, for this layer and scanning line. Upon scanning through the range $[\rho_{xx}^-, \rho_{xx}^+]$, the maximum of all $\lambda_{\rho z}$ is recorded as the load factor for the layer λ_z. This process is repeated for all layers, and the static shakedown limit is obtained by taking the minimum of all λ_z. The above procedure for determining of static shakedown limit can also be found in Krabbenhøft et al. (2007a).

In theory, if the exact elastic stress field is known, the static shakedown limit defined by Eq. (1) can be found as the best of all the lower bounds. This is equivalent to determining the exact shakedown limit. In practice, however, this is often difficult and we must obtain the shakedown limit numerically. The accuracy of such a solution is governed by the discretisation and any additional tolerances. In the following, we employ very fine meshes and tight tolerances to minimise the overall solution error. Even so, what we obtain is essentially a lower bound rather than an exact value for the shakedown limit. In view of this, we described the shakedown limit computed as a 'static shakedown limit'.

Compared to the type 1 and type 2 upper bounds, the determination of type 3 upper bounds is much more difficult. In this case, there are no obvious bounds on the residual stresses to use with the scanning line method when dealing with the equilibrium condition. Where all conics in a layer are ellipses, we can find a pair of bounds, $\hat{\rho}_{xx}^-$ and $\hat{\rho}_{xx}^+$, by determining the maximum of the left-most bounds and the minimum of the right-most
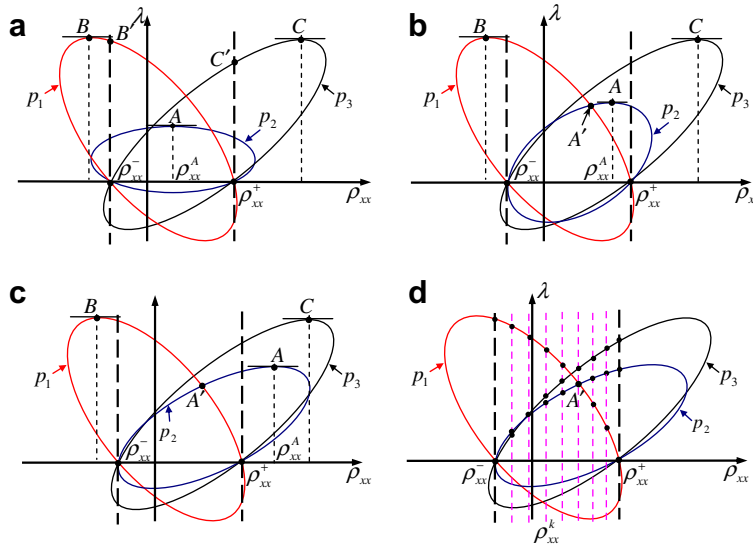
Fig. 5. Determination of static shakedown limit. (a–c) Some typical examples by using the method of conics; (d) by using the scanning line method.

bounds on the residual stresses for all ellipses in each layer (see Fig. 6). The scanning line method can then be applied to calculate the type 3 upper bound. However, in the case where the conics are hyperbolic and/or parabolic, the situation becomes very complicated. Since this case can be found by other means, such as finite element limit analysis formulations, it will not be dealt with here.

In the following computations the contact half-length, a, and the cohesion of the soil, c, will be used to normalise all other variables. This permits the load factor $\lambda p_0/c$ to be used to evaluate the shakedown limit and the two upper bounds. Generally speaking, the critical material point for the shakedown load factor occurs within a small distance of the contact area. Thus a domain of width W and depth D around the contact area is used in the computation. This domain should be large enough to cover all possible critical points, while at the same time being as small as possible to reduce the computational effort when a very fine mesh is used (Fig. 7). Note that a structured mesh is preferred to an unstructured mesh, as it is more convenient for checking the load factor layer by layer. The complete numerical procedure for computing the shakedown load factor is shown in Table 1. The quantities W/a and D/a are, respectively, the normalised width and depth of the domain, while b/a specifies the form of the trapezoidal contact. The quantities n_x and n_z denote the number of nodes in the x and z directions for the mesh, n_ρ is the number of divisions for checking that the residual stress is within the bounds (20), μ is the roller friction coefficient, ϕ is the soil internal friction angle, and TOL denotes a small numerical tolerance.

4.2. Results and discussion

We start with a simulation region that is large enough to include all the critical material points for the initial calculations of the various shakedown load factors. The initial region is chosen to be $x = [-4a, 4a]$ and $z = [0, 4a]$. The simulated area is discretised into 400×200 ($n_x \times n_z$) structured elements as illustrated in Fig. 7. An initial computation is then carried out to roughly locate the critical positions which govern the shakedown load. To accurately determine the shakedown limit, the simulated region is narrowed to include a small area around the critical position while retaining horizontal symmetry (say $x = [-1.25a, 1.25a]$ and $z = [0, 1.25a]$ for example) and another refined mesh (say 800×400) is generated in this area again to compute the shakedown limit. The sensitivity of the shakedown load factors to the mesh resolution as well as simulated region size will be discussed later. For the static shakedown limit, we divide the range of ρ_{xx} defined by Eq. (20) into 400 (n_ρ) segments. The friction coefficient for the roller-road surface is assumed to lie in the range
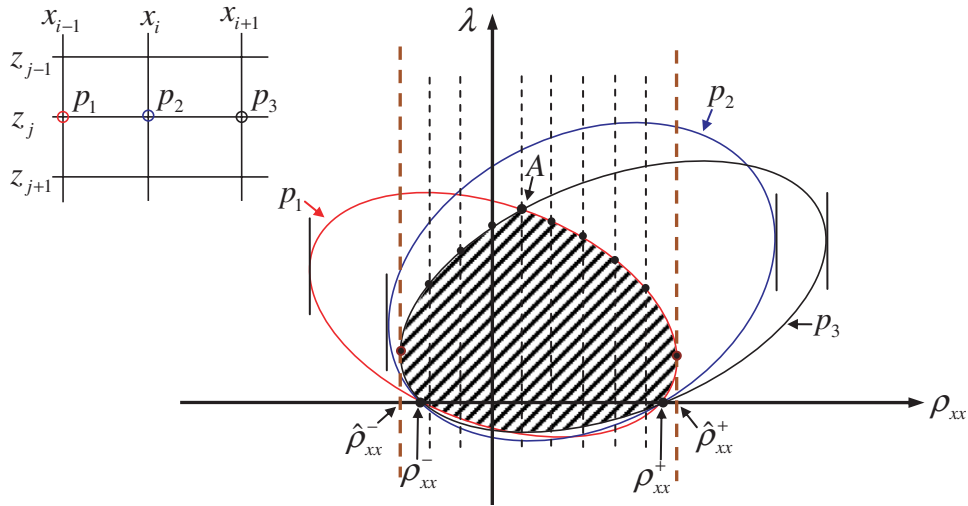
Fig. 6. Illustration of determination of the load factor for upper bound type 3 for special cases where all the conics are ellipses in a layer.
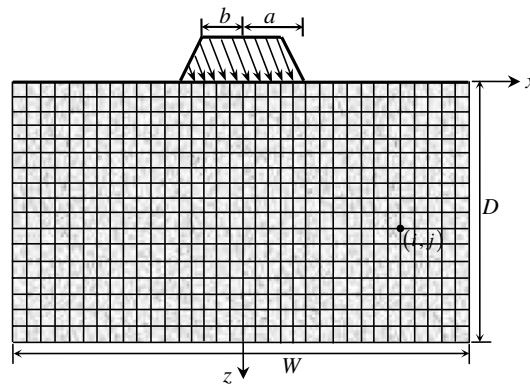

Fig. 7. Illustration of the mesh used for shakedown analysis.

$[0, 1]$, while the internal friction angle of the soil is taken as $0°$, $15°$, $30°$ and $45°$. The tolerance for approximating zero, TOL, is set roughly equal to the machine precision (10^{-16}).

4.2.1. Load factors for shakedown under Hertzian and trapezoidal surface contacts

We first consider trapezoidal contact where the ratio of $b/a = 0.5$ is adopted. Fig. 8 presents the shakedown and elastic limit load factors for both trapezoidal and Hertzian contact, where the latter are due to Krabbenhøft et al. (2007a). Note that the load for the trapezoidal contact has been scaled to the Hertzian case using Eq. (8) so that all the load factors can be expressed in terms of the maximum Hertzian pressure p_0. For future reference, Table 2 also gives the shakedown results for the trapezoidal case in terms of the maximum pressure p_0'.

Some common trends in the load factors can be observed from Fig. 8 for both the Hertzian and trapezoidal contact approximations:

(1) The shakedown load factors decrease rapidly as the roller friction μ increases, and increase markedly with the increasing internal friction angle ϕ (particularly at low μ values). This echoes the earlier findings for frictionless materials of Johnson (1990), Hills and Ashelby (1982) and Ponter et al. (1985), as well as the results for frictional materials of Sharp and Booker (1984), Collins and Cliffe (1987) and Krabbenhøft et al. (2007a). If the friction coefficient μ is small, the critical position for the shakedown factor is subsurface; whereas if μ is large, surface failure becomes critical. In the latter case, the shake-

Table 1
Flow chart for determination of the elastic limit, shakedown limit, upper bound type 1 and type 2

(1) Enter with the parameters: W/a, D/a, b/a, n_x, n_z; n_ρ, μ, ϕ; $TOL^{[a]}$;

(2) Discretise the concerned region into a structured mesh $n_x \times n_z$;

(3) Calculate ρ_{xx}^+ and ρ_{xx}^- according to Eq. (20) and divide $(\rho_{xx}^+ - \rho_{xx}^+)$ into n_ρ steps;

(4) Set $\lambda_{SD} = \lambda_I = \lambda_{II} = \lambda_{III} = 0$;

(5) Loop: $i = 1$ to n_z

    (6) Loop: $j = 1$ to n_x

        (7) Calculate $\sigma_{xx}^{(i,j)}$, $\sigma_{zz}^{(i,j)}$ and $\sigma_{xz}^{(i,j)}$ according to the Hertzian elastic stresses or the trapezoidal ones in (10)-(15).

        (8) Calculate $\alpha_1^{(i,j)} = |\sigma_{xz}^{(i,j)}| - \sigma_{xz}^{(i,j)} \tan \phi$.

        (9) Calculate $\alpha_E^{(i,j)} = \sqrt{(\sigma_{zz}^{(i,j)} - \sigma_{xx}^{(i,j)})^2 + 4(\sigma_{xz}^{(i,j)})^2} - (\sigma_{zz}^{(i,j)} + \sigma_{xx}^{(i,j)}) \sin \phi$

        (10) Calculate $\rho_{xx}^{*(i,j)}$ according to Eqs. (18) and (19).

        (11) If: $\rho_{xx}^{*(i,j)} \geqslant \rho_{xx}^+$ or $\rho_{xx}^{*(i,j)} \leqslant \rho_{xx}^-$

            (12) Let $\rho_{xx}^* = \rho_{xx}^+$ and $\rho_{xx}^* = \rho_{xx}^-$, calculate $\hat{\lambda}_{II}^{(j)+}$ and $\hat{\lambda}_{II}^{(j)-}$ by Eq. (18);

            (13) Determine $\hat{\lambda}_{II}^{(j)} = \max(\hat{\lambda}_{II}^{(j)+}, \hat{\lambda}_{II}^{(j)-})$.

        (14) Else

            (15) Use $\rho_{xx}^{*(i,j)}$ to calculate $\hat{\lambda}_{II}^{(j)}$ according to Eq. (18).

        (16) End-If

    (17) End-Loop

    (18) Determine $\bar{\lambda}_{II}^{(i)} = \min_j \hat{\lambda}_{II}^{(j)}$.

    (19) Loop: $j = 1$ to $(n_\rho + 1)$

        (20) Calculate $\rho_{xx}^{(j)} = \rho_{xx}^- + (j-1)((\rho_{xx}^+ - \rho_{xx}^-)/n_\rho)$;

        (21) Loop over $k = 1$ to n_x

            (22) Substitute $\rho_{xx}^{(j)}$, $\sigma_{xx}^{(i,k)}$, $\sigma_{zz}^{(i,k)}$ and $\sigma_{xz}^{(i,k)}$ into Eq. (17) and solve for λ. If there are two roots for λ: $\hat{\lambda}_{SD}^{(k)_1}$ and $\hat{\lambda}_{SD}^{(k)_2}$, $\hat{\lambda}_{SD}^{(k)} = \max(\hat{\lambda}_{SD}^{(k)_1}, \hat{\lambda}_{SD}^{(k)_2}, 0)$. If there is no root for λ, $\hat{\lambda}_{SD}^{(k)} = \inf$ where inf is a large positive number.

        (23) End-Loop

        (24) Determine $\tilde{\lambda}_{SD}^{(j)} = \min_k \hat{\lambda}_{SD}^{(k)}$;

    (25) End-Loop.

    (26) Determine $\lambda_{SD}^{(i)} = \max_j \tilde{\lambda}_{SD}^{(j)}$;

(27) End-Loop

(28) Calculate $\lambda_I = 1/\max_{(i,j)} \alpha_1^{(i,j)}$; $\lambda_{II} = \min_i \bar{\lambda}_{II}^{(i)}$; $\lambda_E = 2\cos\phi/\max_{(i,j)} \alpha_E^{(i,j)}$, $\lambda_{SD} = \min_i \lambda_{SD}^{(i)}$.

(29) Output λ_{SD}, λ_I, λ_{II} and λ_E.

[a] Note that *TOL* is used in Step (12) and Step (22), even though it is not shown explicitly.

down limit is governed by the range of the elastic stress σ_{xx} and the non-proportional cycle of stress experienced by a surface element of the road. This stress cycle is particularly damaging to the life of a pavement and comprises a tensile stress σ_{xx}, an orthogonal shear stress σ_{xz}, and then a compressive σ_{xx}. The non-smooth point in the static shakedown curve for each ϕ indicates the boundary between surface and subsurface failure in terms of μ. Since μ for the transition point becomes smaller when the internal friction angle ϕ increases, this implies that surface failure is more likely to occur in a frictional soil than in a frictionless one (under the same surface traction).

(2) In both upper bound solutions, there is a non-smooth transition point in the response which indicates a change from subsurface failure to surface failure as the coefficient of friction is increased. This point, however, occurs at a larger value of μ than in the static shakedown case (except for Hertzian contact with $\phi = 0°$, where all three curves coincide). These results highlight the fact that a physically realistic residual stress field will cause significant deformation of the soil in the proximity of the surface. When this effect is combined with an external load that causes large shear stresses, surface failure is easily triggered. For the two upper bounds, relaxing the equilibrium conditions and/or yield constraint on the residual stresses results in soil elements that may deform as rigid bodies, so that more of the surface load is transmitted to deeper elements. This explains why these solutions predict subsurface failure at relatively high friction coefficients.
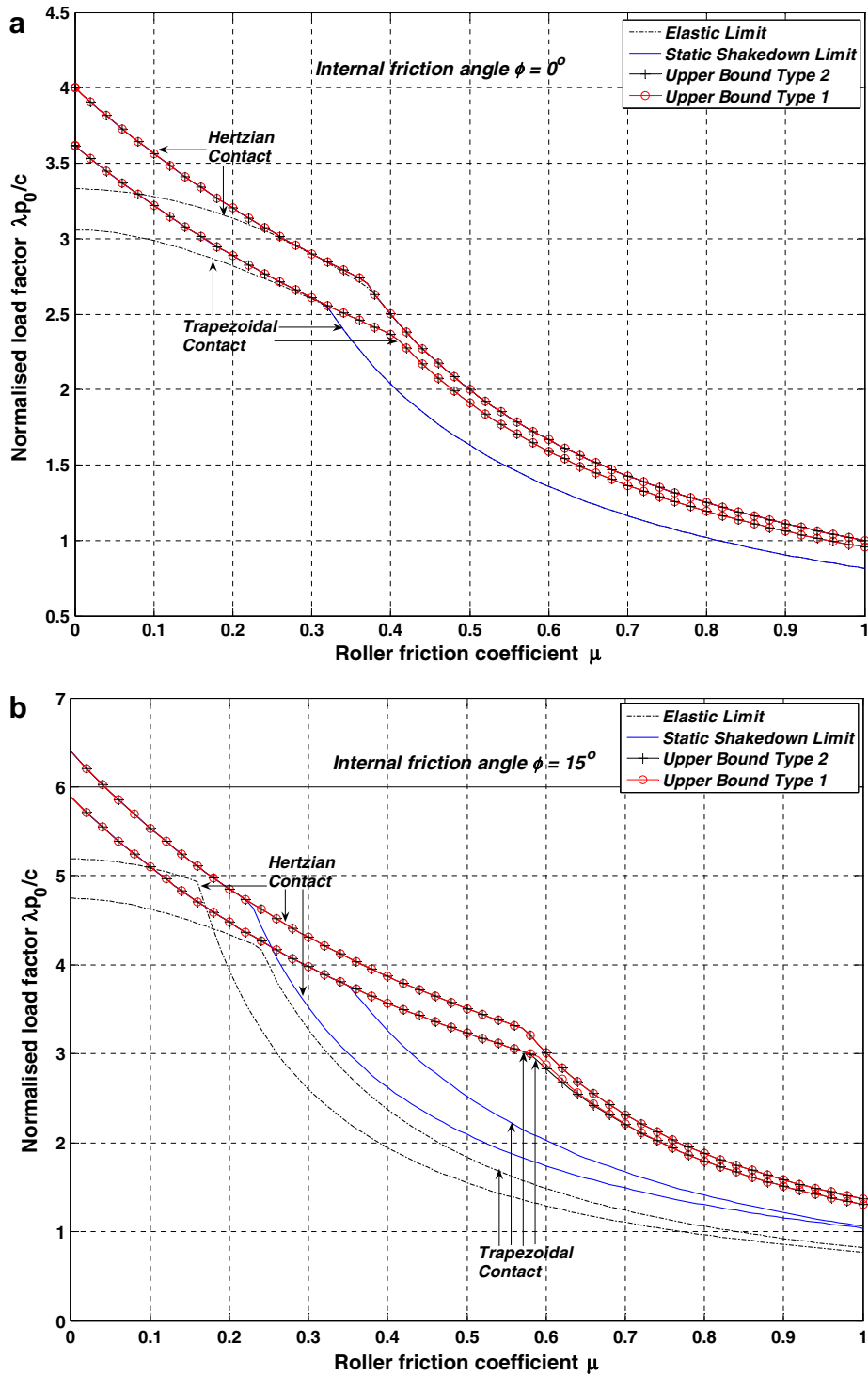
Fig. 8. Load factors for shakedown and elastic limit under Hertzian and trapezoidal contact (a) $\phi = 0°$; (b) $\phi = 15°$; (c) $\phi = 30°$; (d) $\phi = 45°$. Note: the load factors for the trapezoidal case have been normalised by the maximum pressure p_0 for the Hertzian contact with $b/a = 0.5$. If the trapezoidal maximum pressure p'_0 is used for the normalisation, a multiplier of $\pi/3 \approx 1.047$ needs to be applied to the corresponding load factors for the trapezoidal contact case.
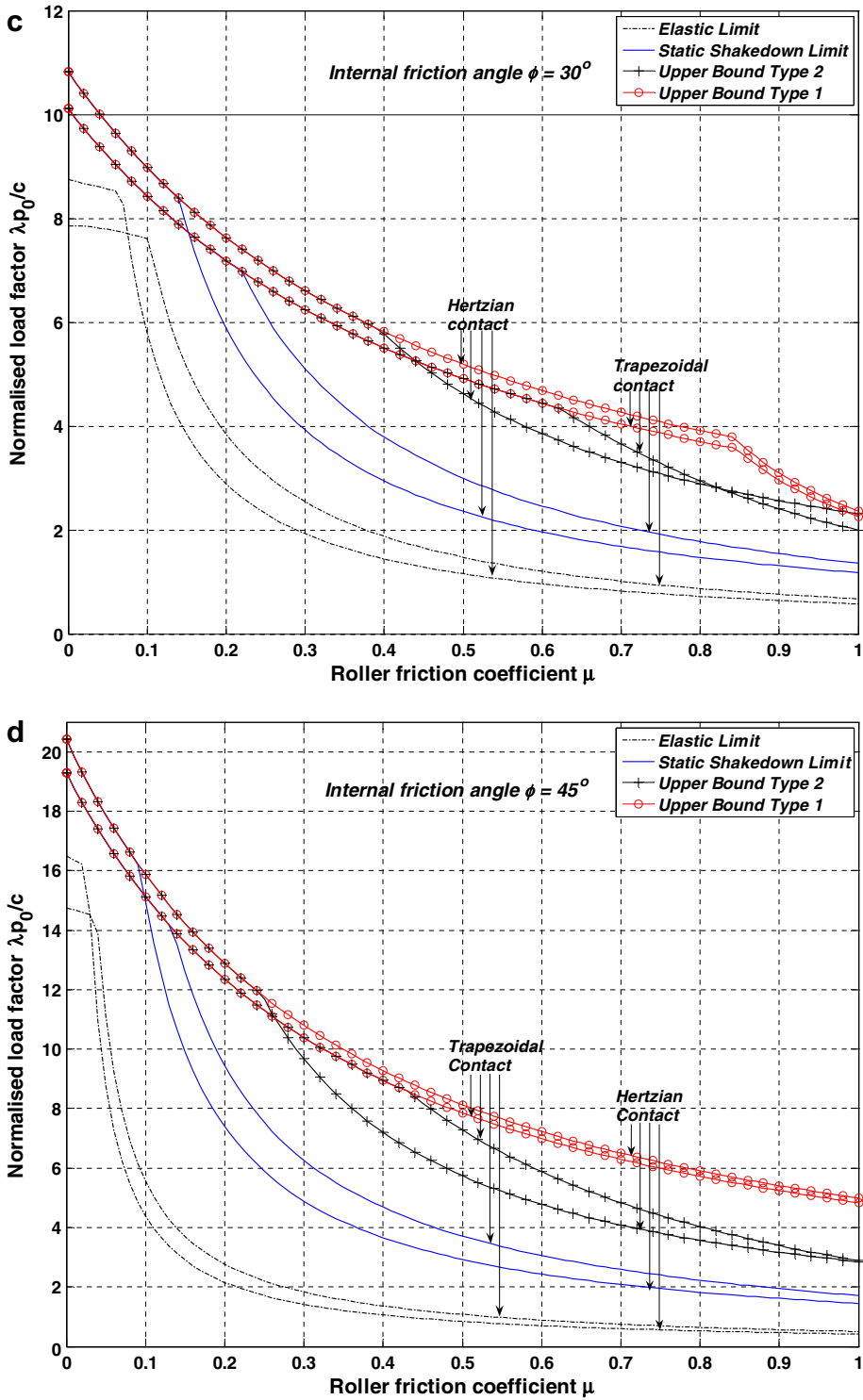
Fig. 8 (*continued*)

(3) The static shakedown limit λ_{SD}, its two upper bounds, λ_I and λ_{II}, and the elastic limit λ_E are such that $\lambda_E \leqslant \lambda_{SD} \leqslant \lambda_{II} \leqslant \lambda_I$ or all cases. For small friction coefficients (for example $\mu \leqslant 0.32$ for the case of $\phi = 0$), subsurface failure is critical and the static shakedown limit coincides with the other two upper bounds. When

Table 2
Shakedown limit load factors, $\lambda p'_0/c$, for a trapezoidal load distribution with $b/a = 0.5$, where p'_0 is the maximum vertical pressure at the centre of the trapezoid

ϕ	$\mu = 0.0$	0.1	0.2	0.3	0.4	0.5	0.6	0.7	0.8	0.9	1
0°	3.789[a]	3.371[a]	3.022[a]	2.729[a]	2.133[b]	1.707[b]	1.422[b]	1.219[b]	1.067[b]	0.948[b]	0.853[b]
15°	6.164[a]	5.341[a]	4.690[a]	4.167[a]	3.420[b]	2.637[b]	2.123[b]	1.750[b]	1.478[b]	1.270[b]	1.110[b]
30°	10.588[a]	8.824[a]	7.523[a]	5.344[b]	3.968[b]	3.133[b]	2.576[b]	2.168[b]	1.862[b]	1.614[b]	1.421[b]
45°	20.193[a]	15.833[a]	9.872[b]	6.578[b]	4.901[b]	3.894[b]	3.210[b]	2.713[b]	2.330[b]	2.036[b]	1.792[b]

[a] Subsurface failure.
[b] Surface failure.

this coefficient increases, the static shakedown limit is the smallest of the three and the type 2 upper bound is better than the type 1 upper bound. Nevertheless, both upper bounds are significantly higher than the static shakedown limit for these cases. For example, with a trapezoidal contact pressure and $\phi = 30°$ and $\mu = 0.7$, the type 1 upper bound and type 2 upper bound are, respectively, 99% and 80% higher than the corresponding static shakedown limit. This suggests that neither of these upper bounds should be used for practical pavement design. It is noteworthy that for frictionless soils where $\phi = 0$, the shakedown limits for the Hertzian and trapezoidal contact conditions coincide with the elastic limit when surface failure dominates.

Fig. 8 shows that there are some major differences between the shakedown limits for the Hertzian and trapezoidal contact cases:

(1) For the same contact length and total pressure, the static shakedown limit for the trapezoidal contact pressure is smaller than its Hertzian counterpart for the frictionless case. When the friction angle is increased, this trend remains true when μ is small and subsurface failures are critical. However, when μ is large and surface failure becomes critical, the trend is reversed with the static shakedown limit for trapezoidal contact being greater. This implies that for frictionless soils like clays, the trapezoidal surface pressure distribution for rolling and sliding contact results in a stress field with larger stress-concentrations than the Hertzian case, and a pavement design based on the former contact approximation is thus more conservative. For frictional soils, the trapezoidal shakedown limit is less than the Hertzian shakedown limit for rollers with small friction coefficients, but becomes greater (and unconservative) when the roller friction coefficient is large.

(2) The transition point from subsurface to surface failure. For Hertzian contact, the transition point occurs at smaller values of μ as the internal friction angle ϕ increases. For the trapezoidal case, this rule does not always apply and we find that for $\phi = 0°$, 15°, 30° and 45°, the corresponding transitional friction coefficients are $\mu = 0.32$, 0.35, 0.22 and 0.13, respectively. Compared to the Hertzian case, the transition value of μ is smaller for the trapezoidal contact case when the soil is frictionless, but larger when the soil is frictional.

Fig. 9 presents a comparison of the new and previous shakedown results. For all four internal friction angles, the new shakedown results for the trapezoidal contact case are very close to those obtained by Sharp and Booker (1984), but vary significantly from those given by Collins and Cliffe (1987). The shakedown loads predicted by the latter are generally smaller than our new results and have no obvious (non-smooth) transition points at all. The reason for this discrepancy is unknown.

4.2.2. Effect of variable trapezoidal shape on the shakedown load factors

We now study the influence of the shape of the trapezoidal pressure distribution, governed by the ratio of b/a, on the shakedown load factor. Five values of b/a are selected for this purpose: $b/a = 0$, 0.3, 0.5, 0.8 and 0.99. The maximum pressure p'_0 and the contact half-length a for the distribution are assumed to be the same for all cases. Fig. 10 shows the computed results for the case $\phi = 30°$.

Results in Fig. 10a are for a normalised load factor that is scaled for trapezoidal contact by $\lambda p'_0/c$ (not by the maximum Hertzian contact pressure p_0). Note that the case of $b/a = 0$ corresponds to a triangular pressure distribution, while the case of $b/a = 0.99$ approximates a rectangular distribution. The exact rectangular case, where $b/a = 1.0$, cannot be modelled due to the occurrence of a stress singularity at the edge of the contact
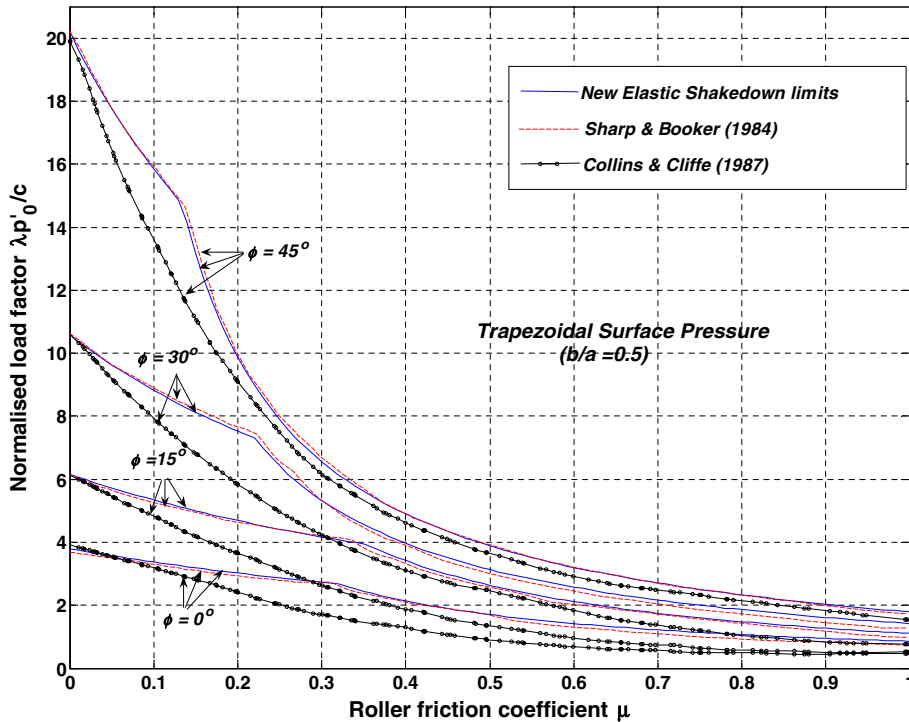
Fig. 9. Comparison of the new elastic shakedown limits with those of Sharp and Booker (1984) and Collins and Cliffe (1987).

area due to the tangential traction (see, also, Johnson, 1985, Fig. 2.9 therein). Fig. 10a shows that as b/a is reduced, the shakedown limit increases and the transition from subsurface to surface failure occurs at larger values of μ for the frictional soils considered. Fixing p'_0 and a, while varying b/a, corresponds to a roller with a different overall load. In view of Fig. 2, larger values of b/a most closely simulate the effects of a tyre under higher load ratio. From Fig. 10a we also see that when b/a approaches 1, the shakedown curve becomes smooth and no obvious non-smooth point identifying the change from subsurface to surface failure is observed.

Alternatively, we can fix the contact half-length and assume the overall force applied to different trapezoidal distributions is the same. By doing this, we can investigate the cyclic bearing capacity for various contact shapes under the same total load. In this case, the maximum pressure for each case will vary according to b/a. To make the various static shakedown limits for all cases comparable, we use the maximum pressure p'_0 for the case of $b/a = 0.5$ as a benchmark, and normalise all load factors with respect to this pressure and the soil cohesion c. The resulting static shakedown limits are shown in Fig. 10b. For the same contact length and overall load, the ratio b/a affects the transition from subsurface to surface failure. The larger the ratio b/a is, the earlier this transition occurs in terms of μ.

It is interesting to note that, in the extreme case when $b/a = 1.0$ and $\mu = 0$ such that the pressure distribution becomes a uniform one and there is no tangential traction, the following analytical solution to the elastic shakedown limit can be found[2]:

$$\lambda^*_{sd} = \frac{p_0}{c} = \frac{\pi}{1 - (\frac{\pi}{2} - \phi) \tan \phi} \tag{21}$$

Fig. 11 presents the variation of this shakedown limit with respect to the frictional angle, compared to the corresponding Hertzian contact case. The above result can serve as a useful benchmark for further numerical shakedown analysis.

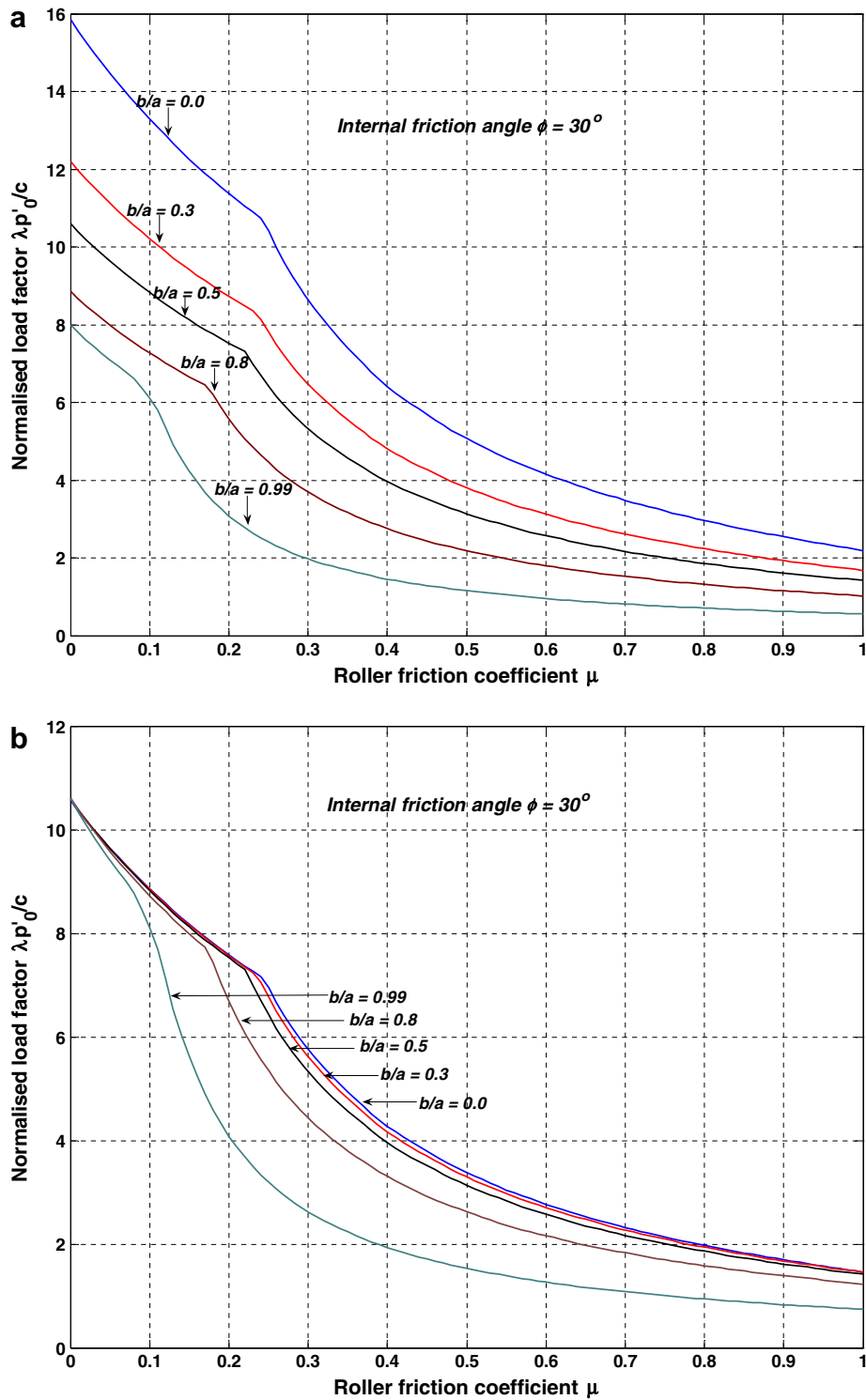[2] This result was provided by the fourth author via personal communication.

Fig. 10. Variation of static shakedown limits to the trapezoidal shape (b/a) for soils with internal friction angle $\phi = 30°$. (a) The various b/a have the same a and the same maximum pressure p'_0. All load factors are normalised by this maximum pressure; (b) all cases have the same a and the same overall load, all the load factors are scaled and normalised by the maximum pressure p'_0 for $b/a = 0.5$.
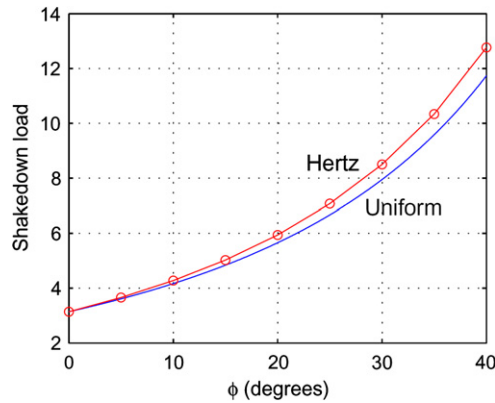
Fig. 11. Shakedown limit under uniform pressure distribution as obtained by Eq. (21).

4.2.3. Sensitivity of shakedown limits to the numerical mesh

Generally speaking, numerical computation of shakedown load factors is highly sensitive to the level of mesh refinement and the accuracy of the stress field. Even when the exact stress field is available, high resolution meshes must be employed to capture the shakedown limit accurately. Moreover, the division of the range bounded by ρ_{xx}^- and ρ_{xx}^+ also has to be sufficiently fine to isolate the optimal residual stress precisely. In passing, we note that the same issues will arise if a discrete finite element method is used to estimate the shakedown limit, especially if a numerical elastic stress field is used to approximate the exact stress field. Indeed, the adoption of very fine meshes can lead to enormous computational effort; not only in the calculation of the stresses, but also in the computation of the shakedown limit using advanced optimisation solvers. To illustrate this point, we consider the trapezoidal contact case. Fig. 12 shows the sensitivity of the shakedown results for $\phi = 30°$. In Fig. 12(a), we first adopt three different regions of simulation: (A) $x = [-4a, 4a]$ and $z = [0, 4a]$; (B) $x = [-2a, 2a]$ and $z = [0, 2a]$; and (C) $x = [-1.25a, 1.25a]$ and $z = [0, 1.25a]$, and discretise them with the same mesh resolutions $(n_x, n_z, n_\rho) = (400, 200, 200)$. Note that the three simulation regions chosen for investigation cover all possible critical locations for both subsurface and surface failures. In Fig. 12(b), we use three different mesh sizes for a simulation region of $x = [-1.25a, 1.25a]$ and $z = [0, 1.25a]$: (A) $(n_x, n_z) = (100, 50)$; (B) $(n_x, n_z) = (200, 100)$; and (C) $(n_x, n_z) = (400, 200)$. Note that n_ρ is fixed in this case to be 200. In Fig. 12(c), we fix the mesh size (n_x, n_z) to be $(400, 200)$ for the region $x = [-1.25a, 1.25a]$ and $z = [0, 1.25a]$, but apply three resolutions of n_ρ to the computation: (A) $n_\rho = 50$; (B) $n_\rho = 100$; and (C) $n_\rho = 200$.

It appears from Fig. 12 that the static shakedown limits are slightly sensitive to the simulation region size, mesh resolution and resolution of the residual stress when surface failure governs, whereas the two upper bound solutions are largely insensitive to these factors for all values of μ. The static shakedown limits are reduced when the simulated region is narrowed, the mesh is refined and surface failure governs. Overall, the shakedown solutions cease to change substantially once the mesh uses a discretisation of $(400, 200)$ together with $n_\rho = 200$. In view of these observations, $(n_x, n_z) = (800, 400)$ and $n_\rho = 400$ were used with a simulation region of $x = [-1.25a, 1.25a]$ and $z = [0, 1.25a]$ to generate the results shown in the previous sections.

5. Conclusions

In this paper, we have considered the application of Melan's theorem to predict the shakedown limit of a cohesive-frictional half space under moving surface load. It shown that, other than the yield constraints on the total stresses, the self-equilibrium and yield constraints on the residual stresses are equally indispensable in deriving rigorous lower bounds. Relaxing one or both of the last two conditions essentially results in various upper bounds to the shakedown limit.

Two pressure distributions for the surface loads are considered, namely Hertzian contact and trapezoidal contact. A new closed form solution for the elastic stress field of a half space under trapezoidal vertical and
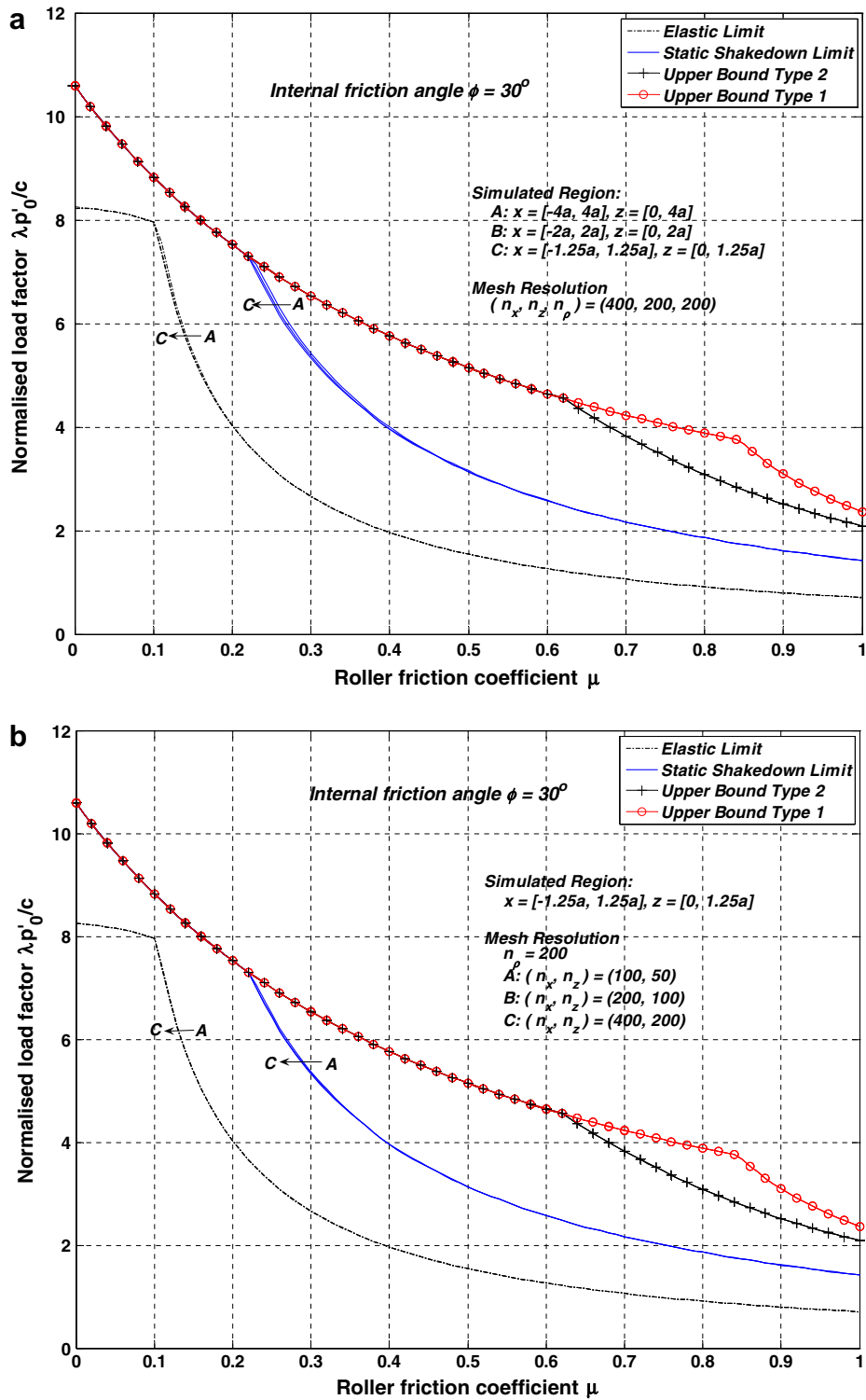
Fig. 12. Sensitivity of shakedown limit and the upper bounds to the (a) simulated region, (b) mesh resolution, and (c) resolution of ρ_{xx}.

horizontal load distributions is obtained. The difference between the static shakedown limit and its various upper bounds for both contact types are demonstrated and comparisons between them have been made.
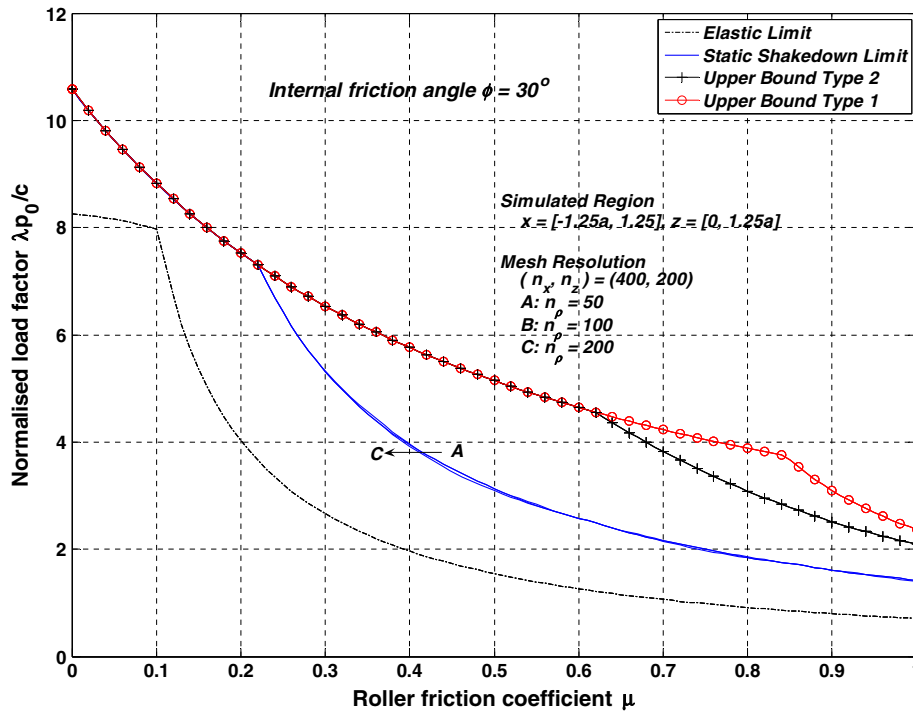
Fig. 12 (*continued*)

The new shakedown limit results derived will be useful in pavement design as well as in benchmarking shakedown solutions obtained from other numerical methods.

Some additional points that are noteworthy are as follows: (1) The contact type discussed in this paper is assumed to be complete slip where the tangential force Q is equal to the limiting friction μP. In the case of partial slip where Q is less than μP, a 'microslip' may occur (Johnson, 1985). Johnson (1990) showed that, for a frictionless material modelled by a Tresca yield criterion, this behaviour will reduce the shakedown limit when surface failure is involved at high friction. (2) Elastic perfectly plastic material behaviour has been assumed in the analyses given in this paper. It is well-known that in such materials, shakedown occurs due to the formation of residual stress fields. The shakedown of material bodies with more complex mechanical behaviour, however, may be caused by additional factors such as microstructural changes (for example, strain hardening) and geometry changes. (3) Two-dimensional plane strain deformation has been assumed for the contact between the roller and the road surface. However, the real contact behaviour is three-dimensional in nature. As remarked by Collins and Cliffe (1987), the plane strain analysis is slightly conservative as it provides smaller shakedown limits than those from three-dimensional elliptical Hertzian contact. This needs to be taken into consideration if the current results are to be used for practical applications. (4) A single homogeneous layer of road material has been considered in this paper. Bitumen pavements, however, are mostly layered structures with several layers of bituminous, rigid and granular materials. The numerical procedure developed here can also be applied to multilayered cases, provided suitably accurate elastic stress fields are available.

Appendix A. Closed form elastic stress solution of half space under Trapezoidal normal pressure and tangential traction

The stress distribution under trapezoidal pressures (in both the vertical and horizontal directions) is obtained using the procedure described in Johnson (1985). The stresses in the $x - z$ half plane induced by

any combination of distributed normal and tangential tractions can be obtained by the following expressions (note that compression is taken as positive here):

$$
\begin{cases}
\sigma_{xx} = \frac{2z}{\pi} \int_{-a}^{a} \frac{p(s)(x-s)^2 \mathrm{d}s}{[(x-s)^2+z^2]^2} + \frac{2}{\pi} \int_{-a}^{a} \frac{q(s)(x-s)^3 \mathrm{d}s}{[(x-s)^2+z^2]^2}, \\
\sigma_{zz} = \frac{2z^3}{\pi} \int_{-a}^{a} \frac{p(s)\mathrm{d}s}{[(x-s)^2+z^2]^2} + \frac{2z^2}{\pi} \int_{-a}^{a} \frac{q(s)(x-s)\mathrm{d}s}{[(x-s)^2+z^2]^2}, \\
\sigma_{xz} = \frac{2z^2}{\pi} \int_{-a}^{a} \frac{p(s)(x-s)\mathrm{d}s}{[(x-s)^2+z^2]^2} + \frac{2z}{\pi} \int_{-a}^{a} \frac{q(s)(x-s)^2 \mathrm{d}s}{[(x-s)^2+z^2]^2}.
\end{cases} \tag{A.1}
$$

where s and ds are depicted in Fig. A.1. Now for the trapezoidal traction distribution, the normal and tangential pressure distribution functions are:

$$
\begin{cases}
p(s) = \frac{s+a}{a-b}p_0, \quad q(s) = \frac{s+a}{a-b}q_0, \quad -a \leqslant s < -b; \\
p(s) = p_0, \quad q(s) = q_0, \quad -b \leqslant s \leqslant b; \\
p(s) = \frac{a-s}{a-b}p_0, \quad q(s) = \frac{a-s}{a-b}q_0, \quad b < s \leqslant a.
\end{cases} \tag{A.2}
$$

where p_0 and q_0 are the maximum normal pressure and horizontal traction, respectively. Substituting Eq. (A.2) into Eq. (A.1), the expressions for the three stresses may be integrated to obtain:

$$
\sigma_{xx} = \frac{p_0}{\pi(a-b)} \left\{ \begin{array}{l} z \ln\left(\left(\frac{(x+b)^2+z^2}{(x+a)^2+z^2}\right)\left(\frac{(x-b)^2+z^2}{(x-a)^2+z^2}\right) \right) + (x+a)\left(\arctan\left(\frac{x+a}{z}\right) - \arctan\left(\frac{x+b}{z}\right)\right) \\ -(x-a)\left(\arctan\left(\frac{a-x}{z}\right) - \arctan\left(\frac{b-x}{z}\right)\right) + (a-b)\left(\arctan\left(\frac{b-x}{z}\right) + \arctan\left(\frac{b+x}{z}\right)\right) \end{array} \right\} \tag{A.3}
$$

$$
+ \frac{q_0}{\pi(a-b)} \left\{ \begin{array}{l} 3z\left(\arctan\left(\frac{x-a}{z}\right) - \arctan\left(\frac{x-b}{z}\right) - \arctan\left(\frac{x+b}{z}\right) + \arctan\left(\frac{x+a}{z}\right)\right) \\ +(x-a)\ln\left(\frac{(x-a)^2+z^2}{(x-b)^2+z^2}\right) - (x+a)\ln\left(\frac{(x+b)^2+z^2}{(x+a)^2+z^2}\right) - (a-b)\ln\left(\frac{(b-x)^2+z^2}{(b+x)^2+z^2}\right) \end{array} \right\}
$$

$$
\sigma_{zz} = \frac{p_0}{\pi} \left\{ \begin{array}{l} \frac{(x+a)}{(a-b)}\left(\arctan\left(\frac{x+a}{z}\right) - \arctan\left(\frac{x+b}{z}\right)\right) + \left(\arctan\left(\frac{b-x}{z}\right) + \arctan\left(\frac{x+b}{z}\right)\right) \\ -\frac{(x-a)}{(a-b)}\left(\arctan\left(\frac{a-x}{z}\right) - \arctan\left(\frac{b-x}{z}\right)\right) \end{array} \right\} \tag{A.4}
$$

$$
+ \frac{zq_0}{\pi(a-b)} \left\{ \left(\arctan\left(\frac{a-x}{z}\right) - \arctan\left(\frac{b-x}{z}\right)\right) - \left(\arctan\frac{x+a}{z} - \arctan\frac{x+b}{z}\right) \right\}
$$

$$
\sigma_{xz} = \frac{zp_0}{\pi(a-b)} \left\{ \left(\arctan\left(\frac{a-x}{z}\right) - \arctan\left(\frac{b-x}{z}\right)\right) - \left(\arctan\frac{x+a}{z} - \arctan\frac{x+b}{z}\right) \right\} \tag{A.5}
$$

$$
+ \frac{q_0}{\pi(a-b)} \left\{ \begin{array}{l} z \ln\left(\left(\frac{(x+b)^2+z^2}{(x+a)^2+z^2}\right)\left(\frac{(x-b)^2+z^2}{(x-a)^2+z^2}\right) \right) + (x+a)\left(\arctan\left(\frac{x+a}{z}\right) - \arctan\left(\frac{x+b}{z}\right)\right) \\ -(x-a)\left(\arctan\left(\frac{a-x}{z}\right) - \arctan\left(\frac{b-x}{z}\right)\right) + (a-b)\left(\arctan\left(\frac{b-x}{z}\right) + \arctan\left(\frac{b+x}{z}\right)\right) \end{array} \right\}
$$

If we employ the notation of Poulos and Davis (1974) and use the following expressions (see Fig. A.1)
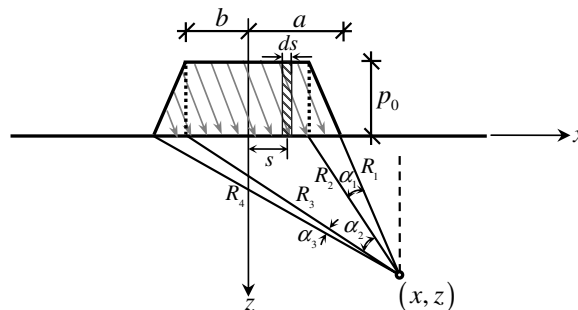

Fig. A.1. Trapezoidal contact.

$$
\begin{cases}
\alpha_1 = \arctan\frac{x-b}{z} - \arctan\frac{x-a}{z}, \quad \alpha_2 = \arctan\frac{x+b}{z} - \arctan\frac{x-b}{z}, \\
\alpha_3 = \arctan\frac{x+a}{z} - \arctan\frac{x+b}{z}, \\
R_1^2 = (x-a)^2 + z^2, \quad R_2^2 = (x-b)^2 + z^2, \\
R_3^2 = (x+b)^2 + z^2, \quad R_4^2 = (x+a)^2 + z^2.
\end{cases}
\tag{A.6}
$$

then the above solution may be rewritten as:

$$
\begin{cases}
\sigma_{xx} = \frac{p_0}{\pi(a-b)}\left\{ z\ln\left(\frac{R_3^2}{R_4^2}\frac{R_2^2}{R_1^2}\right) + (x+a)\alpha_3 - (x-a)\alpha_1 + (a-b)\alpha_2 \right\} \\
\qquad + \frac{q_0}{\pi(a-b)}\left\{ 3z(\alpha_3 - \alpha_1) + (x-a)\ln\left(\frac{R_1^2}{R_2^2}\right) - (x+a)\ln\left(\frac{R_3^2}{R_4^2}\right) - (a-b)\ln\left(\frac{R_2^2}{R_3^2}\right) \right\} \\
\sigma_{zz} = \frac{p_0}{\pi(a-b)}\left\{ (x+a)\alpha_3 + (a-b)\alpha_2 - (x-a)\alpha_1 \right\} + \frac{zq_0}{\pi(a-b)}\left\{ \alpha_1 - \alpha_3 \right\} \\
\sigma_{xz} = \frac{zp_0}{\pi(a-b)}\left\{ \alpha_1 - \alpha_3 \right\} + \frac{q_0}{\pi(a-b)}\left\{ z\ln\left(\frac{R_3^2}{R_4^2}\frac{R_2^2}{R_1^2}\right) + (x+a)\alpha_3 - (x-a)\alpha_1 + (a-b)\alpha_2 \right\}
\end{cases}
\tag{A.7}
$$

The above results can be further simplified to such special cases as triangular and uniform distributions of pressure, for which the reduced solutions can be easily verified to be identical with those presented in Johnson (1985) and Poulos and Davis (1974).

References

Boulbibane, M., Ponter, A.R.S., 2006. The linear matching method for the shakedown analysis of geotechnical problems. Int. J. Numer. Anal. Methods Geomech. 30, 157–179.

Bousshine, L., Chaaba, A., de Saxce, G., 2003. A new approach to shakedown analysis for non-standard elastoplastic material by the bipotential. Int. J. Plast. 19, 583–598.

Brown, S.F., 1996. Soil mechanics in pavement engineering. Géotechnique 46 (3), 383–426.

Collins, I.F., Cliffe, P.F., 1987. Shakedown in frictional materials under moving surface loads. Int. J. Numer. Anal. Methods Geomech. 11, 409–420.

Collins, I.F., Wang, A.P., Saunders, L.R., 1993. Shakedown in layered pavements under moving surface loads. Int. J. Numer. Anal. Methods Geomech. 17, 165–174.

Collins, I.F., Boulbibane, M., 2000. Geomechanical analysis of unbound pavements based on shakedown theory. J. Geotech. Geoenviron. Eng. ASCE 126 (1), 50–59.

Croney, D., 1977. The Design and Performance of Road Pavements. Transport and Road Research Laboratory, London.

Feng, X.Q., Sun, Q.P., 2007. Shakedown analysis of shape memory alloy structures. Int. J. Plast. 23 (2), 183–206.

Freitag, D.R., Green, A.J., 1962. Distribution of stresses on an unyielding surface beneath a pneumatic tyre. Highway Res. Board Bull. 342, 14–23.

Hills, D.A., Ashelby, D.W., 1982. The influence of residual stresses on contact load bearing capacity. Wear 65 (2), 221–240.

Johnson, K.L., 1985. Contact Mechanics. Cambridge University Press.

Johnson, K.L., 1990. A graphical approach to shakedown in rolling contact. In: Hyde, T.H., Ollerton, E. (Eds.), Applied Stress Analysis. Elsevier, pp. 263–274.

Koiter, W.T., 1960. General theorems of elastic–plastic solids. In: Sneddon, J.N., Hill, R. (Eds.), . In: Progress in Solid Mechanics, vol. 1. North-Holland, Amsterdam, pp. 67–221.

König, J.A., 1987. Shakedown of Elastic–Plastic Structures. PWN-Polish Scientific Publishers, Warsaw.

König, J.A., Maier, G., 1981. Shakedown analysis of elastoplastic structures: a review of recent developments. Nucl. Eng. Des. 66, 81–92.

Krabbenhøft, K., Lyamin, A.V., Sloan, S.W., 2007a. Shakedown of a cohesive-frictional half-space subjected to rolling and sliding contact. Int. J. Solids Struct. 44, 3998–4008.

Krabbenhøft, K., Lyamin, A.V., Sloan, S.W., 2007b. Bounds to shakedown loads for a class of deviatoric plasticity models. Comput. Mech. 39, 879–888.

Li, H.X., Yu, H.S., 2006. A non-linear programming approach to kinematic shakedown analysis of composite materials. Int. J. Numer. Methods Eng. 66, 117–146.

Maier, G., 2001. On some issues in shakedown analysis. J. Appl. Mech. ASME 68, 799–808.

Martin, J.B., 1975. Plasticity: Fundamentals and General Results. The M.I.T. Press, Cambridge, MA.

Melan, E., 1938. Zur plastizität des räumlichenkontinuums. Ing. Arch. 9, 116–126.

Pham, D.C., 2007. Shakedown theory for elastic plastic kinematic hardening bodies. Int. J. Plast. doi:10.1016/j.ijplas.2006.11.003.

Polizzotto, C., 1982. A unified treatment of shakedown theory and related bounding techniques. Solid Mech. Arch. 7, 191–275.

Polizzotto, 1993. On the conditions to prevent plastic shakedown of structures: Part II-the plastic shakedown limit load. Trans. ASME 60, 20–25.

Polizzotto, C., 2007. Shakedown theorems for elastic–plastic solids in the framework of gradient plasticity. Int. J. Plast. doi:10.1016/j.ijpla.2007.03.001.

Polizzotto, C., Borino, G., Fuschi, P., 2001. Weak forms of shakedown for elastic–plastic structures exhibiting ductile damage. Meccanica 36, 49–66.

Ponter, A.R.S., Chen, H.F., Ciavarella, M., Specchia, G., 2006. Shakedown analysis for rolling and sliding contact problems. Int. J. Solids Struct. 43, 4201–4219.

Ponter, A.R.S., Hearle, A.D., Johnson, K.L., 1985. Application of the kinematical shakedown theorem to rolling and sliding point contacts. J. Mech. Phys. Solids 33 (4), 339–362.

Poulos, H.G., Davis, E.H., 1974. Elastic Solutions for Soil and Rock Mechanics. John Wiley & Sons, Inc.

Pycko, S., Maier, G., 1995. Shakedown theorems for some classes of nonassociative hardening elastic–plastic material models. Int. J. Plast. 11 (4), 367–395.

Sharp, R.W., Booker, J.R., 1984. Shakedown of pavements under moving surface loads. J. Transport. Eng. ASCE 110 (1), 1–14.

Shiau, S.H., 2001. Numerical methods for shakedown analysis of pavements. Ph.D. thesis, The University of Newcastle, Australia.

Stein, E., Zhang, G., Kôonig, J.A., 1992. Shakedown with nonlinear strain hardening including structural computation using ßnite element method. Int. J. Plast. 8, 1–31.

Symonds, P.S., 1951. Shakedown in continuous media. J. Appl. Mech. ASME 18, 85–89.

Yu, H.S., 2005. Three-dimensional analytical solution for shakedown of cohesive-frictional materials under moving surface loads. Proc. R. Soc. A 461, 1951–1964.

Yu, H.S., Hossain, M.Z., 1998. Lower bound shakedown analysis of layered pavements using discontinuous stress fields. Comput. Methods Appl. Mech. Eng. 167, 209–222.

Zouain, N., Silveira, J.L., 2001. Bounds to shakedown loads. Int. J. Solids Struct. 38, 2249–2266.